The Strongly Controlled Helicopter*

Linghai Lu, Gareth Padfield, and Michael Jump**

Flight Science & Technology Research Group
Department of Engineering
University of Liverpool

Abstract

An investigation into the concept of helicopter stability under flight-path constraint in descending flight is reported in this paper. The research uses the theory of weakly coupled systems to partition the helicopter dynamic system into three interacting subsystems approximating the longitudinal dynamics – the forward speed 'surge' mode, the pitch phugoid mode and the vertical speed 'heave' mode. Under certain conditions, strong control of flight path or vertical speed is shown to drive the aircraft unstable and a conflict exists in feedback gain values to guarantee stability of both the surge and the phugoid modes. Furthermore, this conflict constitutes a potential source of rotorcraft-pilot coupling problems. The problems are exacerbated in autorotation or other cases when the use of collective control is severely restricted. The results from piloted simulations using a FLIGHTLAB Bell412 simulation model have validated the approximate theoretical analysis and are presented in the paper.

List of Symbols

$\mathbf{A}$, $\mathbf{A}_{i,j}$	System matrix and its sub partitioning
k_{w0}	Gain value in feedback from vertical velocity to longitudinal cyclic (deg/m/s)
k_{max}	The maximum gain value for loci plot
K_1, K_2	Critical gains for phugoid mode
q	Pitch rate (rad/sec)
r, R	Maximum and minimum moduli of eigenvalues of $\mathbf{A}_{11}$ and $\mathbf{A}_{22}$, respectively
u, w	Forward and vertical speed in the body axes (ft/sec)
w_0	Vertical velocity (ft/sec)
W_e	Trim vertical speed in the body axes (ft/sec)
U_e	Trim forward speed in the body axes (ft/sec)
V_x, V_z	Forward and vertical speed in the Earth axes (knots)
$\boldsymbol{x}$	State variable vector
γ	Maximum element of $\mathbf{A}_{11}$
γ_d, γ_e,	Desired and deviated flight path angle
δ	Maximum element of $\mathbf{A}_{22}$
λ_i	Eigenvalues of surge and pitch modes
θ, Θ_e	Pitch angle and trim pitch angle (deg)
θ_0, θ_{ls}	Main rotor collective and longitudinal cyclic input (deg)

* Submitted to the 34th ERF, Liverpool, Sept 2008
** Corresponding author **Email:** Linghai@liv.ac.uk

Tel: +44 151 794 8508; **Fax:** +44 151 794 6841

1. Introduction

Interactions between an aircraft and its pilot, commonly described as pilot-induced oscillations or aircraft-pilot couplings (PIOs, APCs), have been investigated extensively since the Wright Brothers experienced such phenomena in their first powered flights [1-4]. Such dynamic couplings often occur when a pilot increases the gain in a closed loop task, working hard to achieve precision. Unfavourable, or adverse, APCs are often sudden or unexpected. It is often difficult to pinpoint the cause of such events and they may lead to extreme outcomes such as loss of aircraft control [5]. The term PIO is limited and arguably, misleading, since the coupling pattern between the aircraft and pilot can, in practice, be either oscillatory or aperiodic. The latter refers to situations where the excursions of aircraft motion diverge monotonically over time rather than oscillate. Therefore, the combined dynamics between the aircraft and pilot are better described as aircraft-pilot coupling (APC) and the consequences are APC events [1, 5]. If rotorcraft are considered, the couplings are described as rotorcraft-pilot coupling (RPCs, [6-10]), and are the subject of this paper.

It is well understood that APC events may be triggered under a variety of circumstances, even

though the nature of the APC might itself be obscure. In Ref. 1, McRuer describes APCs in three categories;

- Cat. I governed by linear behaviour of the pilot and system. The couplings are normally associated with high gain and increased time or phase delay effects.
- Cat. II typically involve limit cycle oscillations of the pilot-vehicle system due to nonlinear control elements in the feedback system, e.g. rate and position saturation.
- Cat. III covers severe pilot-vehicle oscillations, which are inherently non-linear and characterised by a transition from one transient response to another.

The search for robust design solutions that mitigate the adverse effects remains a current research topic. The present paper addresses Cat. I RPCs, where the physical origins and design solutions are linked through an understanding of control strategy. Digital fly-by-wire flight control systems can, if not carefully designed, increase the potential for adverse interactions due to transport delays; nonlinearities in rate and position limiter elements, flight-path constraints, or response type transition effects are other sources of adverse couplings. Pilot errors of judgement resulting from mildly adverse APCs can contribute to the development of more severe APC events.

Under high gain situations such as air refuelling, target tracking, operations in confined areas in poor visibility, or in the presence of disturbed atmospheric conditions, the aircraft needs to operate under attitude and flight-path constraint [9]. Modern aircraft can be designed to deal with these kinds of situations through the stability and control augmentation system (SCAS). However, the coupled system - aircraft, SCAS and pilot - may show unexpected stability characteristics such that strong control of one part of the system may drive another part unstable; hence the need to address this topic of 'stability under constraint' analytically.

The pioneers Neumark [12] and Pinsker [13] investigated the problem of longitudinal stability of fixed wing aircraft under constraint. In [14] Milne and Padfield extended Neumark's seminal work establishing a sound theoretical basis for such analysis, forming the foundation for the present work. In [15] a study, confined to linear dynamic models, was undertaken to determine whether longitudinal low order equivalent system parameters could be used to predict PIOs. Hess and Kalteis [16] employed the optimal control model to investigate the susceptibility of an aircraft to longitudinal PIOs in pitch attitude tracking tasks.

The focus of the present study is an investigation of rotorcraft stability under flight-path constraint, particularly in situations where the use of collective pitch is restricted. The investigation aims to provide a theoretical framework for predicting Cat. I RPC problems; the method is applied to the longitudinal stability of the FLIGHTLAB Bell 412, a model that has received extensive validation work at Liverpool [17]. The stability of the closed-loop system is analysed by dividing the whole system into three sub-modes: the surge (forward speed) mode, the pitch phugoid mode, and the heave (vertical speed) mode, using the theory of the weakly coupled system (WCS) [14, 18]. While the work does not address specific problems encountered by actual rotorcraft, it does explore the potential for RPCs generically.

The paper is structured as follows; after the brief introduction to the theory and problem in Sections 2 and 3, different partitioning levels using WCS theory are explored in Section 4. A stability analysis of the surge mode and pitch phugoid mode is presented in Section 5, and finally, the results from piloted simulation are discussed in Section 6.

2. The theory of weakly coupled dynamic systems

A linear homogeneous dynamic system may be described by equations of the form:

$$\dot{\boldsymbol{x}} = \mathbf{A}\boldsymbol{x} \tag{1}$$

where the vector $\boldsymbol{x} \in \mathbb{R}^m$ is the state variable vector and $\mathbf{A} \in \mathbb{R}^{m \times m}$ is a square, real, and constant matrix. The system in Eq. (1) is partitioned into the form as follows:

$$\begin{bmatrix} \dot{\boldsymbol{x}}_1 \\ \dot{\boldsymbol{x}}_2 \end{bmatrix} = \left[\begin{array}{c:c} \mathbf{A}_{11} & \mathbf{A}_{12} \\ \hdashline \mathbf{A}_{21} & \mathbf{A}_{22} \end{array}\right] \begin{bmatrix} \boldsymbol{x}_1 \\ \boldsymbol{x}_2 \end{bmatrix} \tag{2}$$

where the vectors $\boldsymbol{x}_1 \in \mathbb{R}^p$ and $\boldsymbol{x}_2 \in \mathbb{R}^q$ are the sub state variable vectors, and the matrices $\mathbf{A}_{i,j}$ have the corresponding dimensions. Particularly, let r and R stand for the maximum and minimum moduli of eigenvalues of the matrices $\mathbf{A}_{11}$ and $\mathbf{A}_{22}$, respectively. Then, the eigenvalues of $\mathbf{A}_{11}$ lie on or within the circle of radius r and those of $\mathbf{A}_{22}$ lie without the circle of radius R.

A system can be termed as a weakly coupled system if the following two conditions are satisfied:

a.) $r/R \ll 1$ (3)

b.) $p\gamma\delta/R^2 \ll 1$ (4)

where γ and δ in Eq. (4) are the maximum elements of $\mathbf{A}_{11}$ and $\mathbf{A}_{22}$ respectively. If these two conditions are held, the eigenvalues of the system in Eq. (1) can be approximated by calculating the eigenvalues of the following two matrices [9, 14, and 18].

$$\mathbf{A}_{11}^{*} = \mathbf{A}_{11} - \mathbf{A}_{12}\mathbf{A}_{22}^{-1}\mathbf{A}_{21} \tag{5}$$

$$\mathbf{A}_{22}^{*} = \mathbf{A}_{22} \tag{6}$$

In addition, a similar process can be constructed for the three-level partitioning,

$$\begin{bmatrix} \dot{\boldsymbol{x}}_1 \\ \dot{\boldsymbol{x}}_2 \\ \dot{\boldsymbol{x}}_3 \end{bmatrix} = \begin{bmatrix} \mathbf{A}_{11} & \mathbf{A}_{12} & \mathbf{A}_{13} \\ \mathbf{A}_{21} & \mathbf{A}_{22} & \mathbf{A}_{23} \\ \mathbf{A}_{31} & \mathbf{A}_{32} & \mathbf{A}_{33} \end{bmatrix} \begin{bmatrix} \boldsymbol{x}_1 \\ \boldsymbol{x}_2 \\ \boldsymbol{x}_3 \end{bmatrix} \tag{7}$$

so that the eigenvalues of the complete system can be approximated by calculating the eigenvalues of the following matrices.

$$\mathbf{A}_{11}^{*} = \mathbf{A}_{11} - [\mathbf{A}_{12} \quad \mathbf{A}_{13}] \begin{bmatrix} \mathbf{A}_{22} & \mathbf{A}_{23} \\ \mathbf{A}_{32} & \mathbf{A}_{33} \end{bmatrix}^{-1} \begin{bmatrix} \mathbf{A}_{21} \\ \mathbf{A}_{31} \end{bmatrix} \tag{8}$$

$$\mathbf{A}_{22}^{*} = \mathbf{A}_{22} - \mathbf{A}_{23}\mathbf{A}_{33}^{-1}\mathbf{A}_{32} \tag{9}$$

$$\mathbf{A}_{33}^{*} = \mathbf{A}_{33} \tag{10}$$

These approximations will form the basis of the search for solutions to RPC Cat. I problems.

3. Flight path constraint in the vertical plane

The homogeneous form of the linearised equations of helicopter motion from rectilinear flight can be written in the form shown in Eq. (11), [9]. In addition, the vertical velocity w_0 reference to the Earth axis is given by the expression in Eq. (12)

Transforming Eq. (11) to include the vertical velocity state variable gives Eq. (13). This transformation allows an investigation of flight path and vertical velocity control to be more easily undertaken.

Proportional pilot feedback control between vertical velocity and longitudinal cyclic can be written as the control law shown in Eq. (14). After rearranging the longitudinal mode into the form described in Eq. (15) and ignoring some small terms, this can be further simplified into the form in Eq. (16). The selected partitioning will be explained later in the paper.

$$\frac{d}{dt}\begin{bmatrix} u \\ w \\ q \\ \theta \end{bmatrix} = \begin{bmatrix} X_u & X_w & X_q - W_e & -g\cos\Theta_e \\ Z_u & Z_w & Z_q + U_e & -g\sin\Theta_e \\ M_u & M_w & M_q & 0 \\ 0 & 0 & 1 & 0 \end{bmatrix} \begin{bmatrix} u \\ w \\ q \\ \theta \end{bmatrix} + \begin{bmatrix} X_{\theta_{ls}} \\ Z_{\theta_{ls}} \\ M_{\theta_{ls}} \\ 0 \end{bmatrix} \theta_{ls} \tag{11}$$

$$w_0 = w - U_e\theta \tag{12}$$

$$\frac{d}{dt}\begin{bmatrix} u \\ w_0 \\ w \\ q \end{bmatrix} = \begin{bmatrix} X_u & g\cos\Theta_e/U_e & X_w - g\cos\Theta_e/U_e & X_q - W_e \\ Z_u & g\sin\Theta_e/U_e & Z_w - g\sin\Theta_e/U_e & Z_q \\ Z_u & g\sin\Theta_e/U_e & Z_w - g\sin\Theta_e/U_e & Z_q + U_e \\ M_u & 0 & M_w & M_q \end{bmatrix} \begin{bmatrix} u \\ w_0 \\ w \\ q \end{bmatrix} \tag{13}$$

$$\theta_{ls} = k_{w_0} w_0 \tag{14}$$

$$\frac{d}{dt}\begin{bmatrix} u \\ w \\ q \\ w_0 \end{bmatrix} = \begin{bmatrix} X_u & X_w - g\cos\Theta_e/U_e & X_q - W_e & X_{\theta_{ls}}k_{w_0} + g\cos\Theta_e/U_e \\ Z_u & Z_w - g\sin\Theta_e/U_e & Z_q + U_e & Z_{\theta_{ls}}k_{w_0} + g\sin\Theta_e/U_e \\ M_u & M_w & M_q & M_{\theta_{ls}}k_{w_0} \\ Z_u & Z_w - g\sin\Theta_e/U_e & Z_q & Z_{\theta_{ls}}k_{w_0} + g\sin\Theta_e/U_e \end{bmatrix} \begin{bmatrix} u \\ w \\ q \\ w_0 \end{bmatrix} \tag{15}$$

$$\frac{d}{dt}\begin{bmatrix} u \\ w \\ q \\ w_0 \end{bmatrix} = \left[\begin{array}{c:c:c:c} X_u & X_w - g\cos\Theta_e/U_e & X_q - W_e & g\cos\Theta_e/U_e \\ \hdashline Z_u & Z_w & U_e & Z_{\theta_{ls}}k_{w_0} \\ \hdashline M_u & M_w & M_q & M_{\theta_{ls}}k_{w_0} \\ \hline\hline Z_u & Z_w & 0 & Z_{\theta_{ls}}k_{w_0} \end{array}\right] \begin{bmatrix} u \\ w \\ q \\ w_0 \end{bmatrix} \tag{16}$$

4. The loci of eigenvalues with different partitioning levels

4.1 The loci for the 'exact' system

The basis of comparisons will be the eigenvalues of the 'exact' system matrix, given in Eq. (1), and illustrated in Figs. 1 and 2. The cases investigated are for trimmed forward speeds V_x = 20 to 50 kts with descending speeds V_z = 0, 5, 10 and 15 kts. In addition, the gain value (k_{w0}, deg/(m/s)) varies from zero to infinity. Because of the similarities of the results, only two typical cases with V_x = 30 kts and V_x = 50 kts are shown.

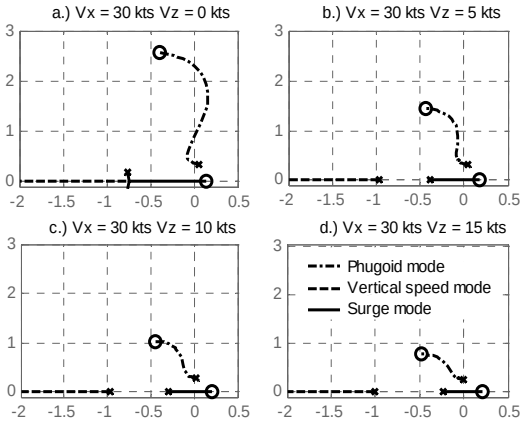

Fig. 1 Eigenvalue loci of the descending Bell 412 helicopter (exact matrix calculation); x – open loop pole; o – closed loop zero

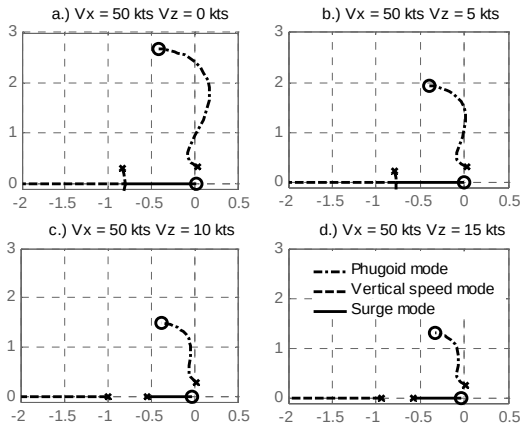

Fig. 2 Eigenvalue loci of the descending Bell 412 helicopter (exact matrix calculation)); x – open loop pole; o – closed loop zero

Figs. 1 and 2 show the eigenvalue loci for the three modes – the pitch phugoid, the surge mode, and the heave mode. Firstly, for the same forward speed, the loci of the phugoid mode are shifted further left as the descending speed increases. The mode tends to be controlled more effectively when the descending speed is higher. For example, the phugoid mode in Fig. 2c is completely moved to the stable plane. In the case of the same descending speed, the phugoid mode is located further right as the forward speed increases. For instance, the loci in Fig. 2b are closer to the imaginary axis compared with Fig. 1b. Secondly, the stability of the surge mode decreases as pilot gain is increased. The locus of this mode moves further right as the descending speed increases for the same forward speed. Moreover, the cases of the same descending speed show more stable results in that the loci move further left as the forward speed increases. Finally, all cases show that the vertical heave speed mode remains stable, demonstrating the effectiveness of the feedback control. However, the control has driven the 'uncontrolled' states into various degrees of instability, revealing a classical RPC.

The curves in Figs. 1a and 2a show a curious phenomenon - the phugoid mode moves first to the left-half plane, and then back to the right-half plane again as the gain is increased further. When the gain value is large enough, the mode is driven stable again. The physical source of these changes in stability is explored in this paper. In the current application, cyclic pitch is used to achieve both flight path control and speed/attitude control. In practice, it is more normal, at low speed, for the pilot to adopt a strategy that uses collective for flight path control and cyclic for attitude/speed control. The analysis that follows is therefore applicable to practical cases of partial power descents with collective malfunction or autorotation flight.

As shown in Figs. 1 and 2, when the feedback gain is large enough, the surge mode is driven increasingly unstable. However, to achieve the stability of the phugoid mode the gain value needs to be reasonably high. There exists a conflict between the control of the speed and pitch attitude and, consequently, the gain value needs to be balanced. This represents a situation that can trigger an RPC. In Refs [12-14] the speed stability problem for fixed-wing aircraft was attributed to strong control of vertical speed when flying below minimum

drag speed. The root cause here being the non-minimum phase characteristic of flight path control with elevator, combined with the fact that drag decreases as speed increases (and vice-versa). A weakly coupled systems analysis, with three-level partitioning of the system dynamics, will be used to explain the curious behaviour of rotary-wing aircraft.

4.2 Eigenvalue loci from a three-level WCS analysis

A three-level analysis, introduced in Section 2, is used to partition Eq. (16). The cases being studied are as same as in Section 4.1 with two representative cases, V_x = 30 kts and V_x = 50 kts, plotted in Figs. 3 and 4.

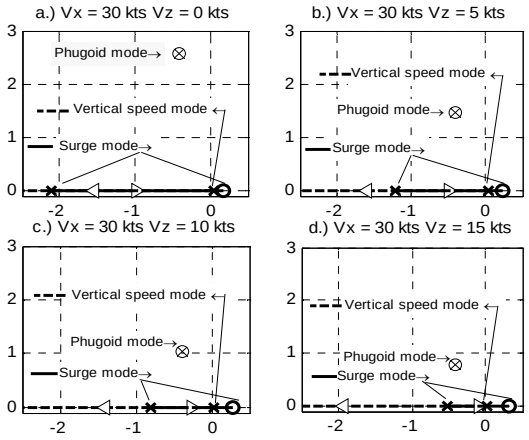

Fig. 3 Eigenvalue loci of the descending Bell 412 helicopter (3-level approximation); x – open loop pole; o – closed loop zero

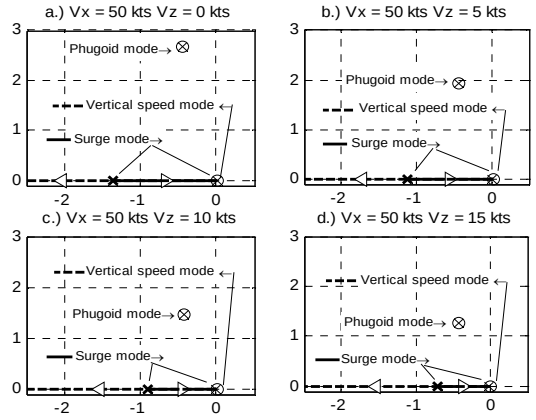

Fig. 4 Eigenvalue loci of the descending Bell 412 helicopter (three-level approximation) ; x – open loop pole; o – closed loop zero

The results shown in these two figures are clearly quite different from those in Figs. 1 and 2. The first difference is the overlapping of the heave and surge mode loci that are shown as the solid line between two poles (the crosses) in the *x*-axes. The second is that the phugoid mode is represented by the closed loop zero from the exact case. This phenomenon can be understood by approximating this mode by the high order sub-system from Eq. (16), given by the following equation [cf. Eq. (10)],

$$\lambda_2^2 - M_q \lambda_2 + M_{\theta_{ls}} = 0 \tag{17}$$

with the additional assumptions:

$$\left| M_{\theta_{ls}} \right| \gg \left| U_e M_w \right| \tag{18}$$

$$\left| Z_{\theta_{ls}} \right| \approx \left| U_e Z_w \right| \tag{19}$$

The loss of speed stability is predicted by this approximation as shown in Fig. 3 and an expression for the critical gain will be developed in Section 5.

4.3 Eigenvalue loci from the 2-level WCS analysis

As discussed in Section 4.2, the three-level analysis failed to predict the low gain behaviour of the phugoid mode. An alternative partitioning of Eq. (16) is given by the two-level system presented in Eqns. (2) and (16). This form of partitioning draws on the low frequency approximations extending from the open loop case [9]. Again, only two cases V_x = 30 kts and V_x = 50 kts are shown in Figs. 5 and 6. The frequency scale in these figures has been reduced to highlight the low frequency behaviour.

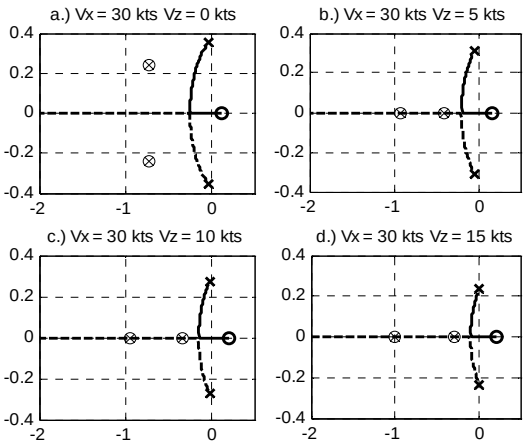

Fig. 5 Eigenvalue loci for the descending Bell 412 helicopter (two-level partitioning); x – open loop pole; o – closed loop zero

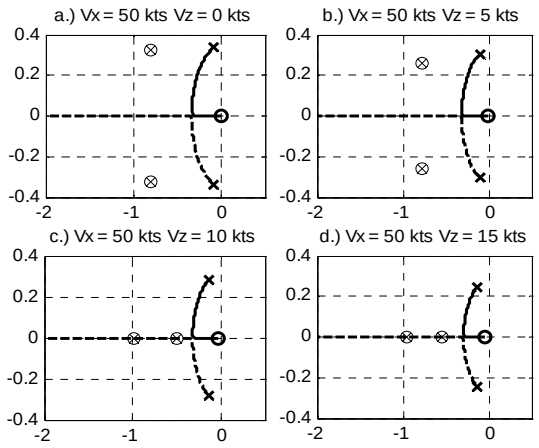

Fig. 6 Eigenvalue loci of the descending Bell412 helicopter (two-level partitioning) ; x – open loop pole; o – closed loop zero

The approximate loci are represented by Eqns. (5) and (6). As shown, the phugoid disappears as the gain value is increased. The open loop values are actually very close to those in Figs. 1 and 2. One interesting point is that, after the break, one root tends to instability (surge mode, solid line), while the second becomes more stable. Figs. 5 and 6 also show the constant eigenvalues from the high modulus sub-system $\mathbf{A}_{22}^{*}$. As with the case of phugoid mode, the starting values are again similar to the corresponding 'exact' modes in Figs. 1 and 2.

The two-level partitioning therefore fails to capture the higher frequency behaviour and the root cause stems from the WCS conditions in Eqns. (3) and (4). As the gain increases, on the one hand the modes move closer together and on the other, the coupling terms in the matrix $A_{12}A_{22}^{-1}A_{21}$ increase in magnitude.

5. Analysis of stability

5.1 Stability of the speed/surge mode

The high-gain, three-level partitioning predicts the low modulus speed mode given by the expression

$$\lambda_1 = X_u + \frac{g[M_u Z_w - Z_u(M_w + M_{\theta_{ls}} k_{w_0})]}{(M_w Z_{\theta_{ls}} - M_{\theta_{ls}} Z_w) U_e k_{w_0}} + \frac{X_w U_e(-M_u Z_{\theta_{ls}} + Z_u M_{\theta_{ls}}) + g M_u Z_{\theta_{ls}}}{(M_w Z_{\theta_{ls}} - M_{\theta_{ls}} Z_w) U_e} \quad (20)$$

Further simplification can be made by examining the relative magnitudes of the stability and control derivatives. For example, the direct derivative terms $M_{\theta_{ls}}$ and Z_w are more significant than $Z_{\theta_{ls}}$ and M_w. The following inequality is generally satisfied,

$$\left|M_{\theta_{ls}} Z_w\right| \gg \left|M_w Z_{\theta_{ls}}\right| \quad (21)$$

For the case of V_x = 45 kts and $V_z = 5$ kts, the value of $\left|M_{\theta_{ls}} Z_w\right|$ is two orders of magnitude larger than $\left|M_w Z_{\theta_{ls}}\right|$. In addition, the following two inequalities are also generally true,

$$\left|M_{\theta_{ls}} Z_w\right| \gg \left|X_w(M_u Z_{\theta_{ls}} - Z_u M_{\theta_{ls}})\right| \quad (22)$$

$$\left|M_{\theta_{ls}} Z_w U_e\right| \gg \left|g M_u Z_{\theta_{ls}}\right| \quad (23)$$

Applying these further approximations, Eq. (20) can be reduced to the expression [9],

$$\lambda_1 = X_u - \frac{g[M_u Z_w - Z_u(M_w + M_{\theta_{ls}} k_{w_0})]}{M_{\theta_{ls}} Z_w U_e k_{w_0}} \quad (24)$$

For the surge mode to be stable, the condition $\lambda_1 < 0$ has to be satisfied. The force derivative Z_u is usually negative at low speed (thrust increases with speed perturbation). Therefore, $\lambda_1 < 0$ can be given by the following inequality,

$$X_u U_e Z_w k_{w_0} M_{\theta_{ls}} - g[M_u Z_w - Z_u(M_w + M_{\theta_{ls}} k_{w_0})] > 0 \quad (25)$$

Applying the further simplifications to establish the core effect,

$$\left|M_u Z_w\right| \gg \left|Z_u M_w\right| \quad (26)$$

$$\left|\frac{g}{U_e} Z_u\right| \gg \left|X_u Z_w\right| \quad (27)$$

Eq. (25) can finally be rewritten as

$$k_{w_0} < \frac{M_u Z_w}{Z_u M_{\theta_{ls}}} \tag{28}$$

In Ref. [14], the corresponding expression for the fixed-wing counterpart to Eq. (24) is given by the approximation,

$$\lambda_{surge} \approx X_u + g\frac{Z_u M_w}{Z_w M_\eta} \tag{29}$$

The M_u effect is very strong at low speed for rotorcraft but is negligible for subsonic fixed wing aircraft. The manner in which the stability problem develops is similar but the underlying effect quite different. The closed loop zero for the approximate surge mode for fixed and rotary wing aircraft is the same however, and given by Eq. (29) (M_η replaced by $M_{\theta_{ls}}$).

The validity of the approximation given in Eq. (28) can be established by comparison with the critical gain values calculated from the exact system (Eq. (16)). The results are shown in Fig. 7.

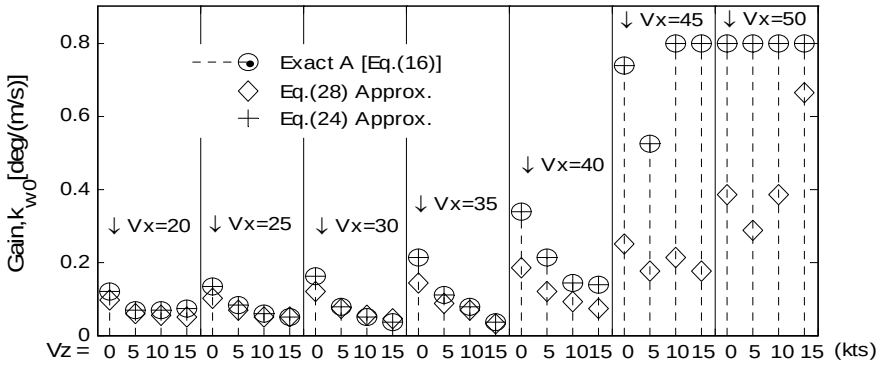

Fig. 7 Comparison of the critical gain values from different approximations (k_{max}= 0.8 deg/(m/s))

In Fig. 7 the term k_{max} is the maximum gain value used to plot the figure. This figure shows that the simple approximation with Eq. (28) predicts the stability boundary very well for forward speeds below 45 kts, demonstrating the effectiveness of the 3-level partitioning. However, at the higher speeds, the approximate predictions diverge from the exact values. Nevertheless, Eq. (24) still remains a good approximation and consequently will be used in analysis that is more general.

Table 1 Critical gains for surge mode (three-level partitioning) k_{w0} (deg/m/s)

$V_z \backslash V_x$	20 kts	25 kts	30 kts	35 kts	40 kts	45 kts	50 kts
0 kts	0.3941	0.4269	0.5254	0.6895	1.1161	2.4287	--
5 kts	0.2200	0.2629	0.2629	0.3613	0.6895	1.7396	--
10 kts	0.2200	0.1972	0.1644	0.2629	0.4598	--	--
15 kts	0.2200	0.1644	0.1316	0.1316	0.4598	--	--

Note: -- mode remains s stable as the gain increases.

The critical gain values of the surge mode from the three-level partitioning are shown in Table 1 (k_{max} = 131.23). They all lie within 5% of the 'exact' values. As V_x increases, the gain value required to destabilise the surge mode also increases. For the case of V_x = 50 kts, the surge mode remains practically stable.

The speed instability is ultimately caused by the same effect as with fixed wing aircraft although the rotor downwash rather than wing downwash is the concern. In the speed range between hover and 50 kts the rotor inflow reduces at its sharpest rate. A positive perturbation in forward speed therefore results in a reduction in inflow and an increase in rotor

thrust. If a pilot pushes forward on the stick to increase descent rate, the speed increases and the increased thrust will eventually cause the aircraft to climb. The M_u effect complicates the situation since a positive speed perturbation causes the rotor disc to flap back and the helicopter to pitch up (this does not happen with fixed-wing aircraft), which tends to reduce the speed. This apparent speed stability is actually the cause of the open loop phugoid instability and it is therefore no surprise that the stability of the surge and phugoid modes are linked under closed loop control.

5.2 Stability of the phugoid mode

The loci of the phugoid mode in Figs. 1a and 2a present a curious phenomenon in that they move back and forth in the complex plane. The approximations derived from the 3-level partitioning predict the closed loop zero correctly and those from the 2-level partitioning predict the modal behaviour at very low gain. The multiple stability crossings, linked as discussed with the changing stability of the surge mode, are not predicted by either of these partitioning. Some insight into the problem can be gained from an examination of the combined medium and high modulus sub-systems in the 3-level partitioning. The problem can then be approached qualitatively by focusing on three degrees of freedom (u, w, q) [see Eq. (16), the solid line].

After using Eq. (5) and then rearrangement, the matrix for the combined phugoid and surge modes is given by Eq. (30).

$$\begin{bmatrix} X_u - 1/(k_{w_0} Z_{\theta_{ls}}) \cdot g / U_e Z_u & X_w - g/U_e - 1/(k_{w_0} Z_{\theta_{ls}}) \cdot g / U_e Z_w & X_q - W_e \\ 0 & 0 & U_e \\ M_u - 1/Z_{\theta_{ls}} \cdot M_{\theta_{ls}} Z_u & M_w - 1/Z_{\theta_{ls}} \cdot M_{\theta_{ls}} Z_w & M_q \end{bmatrix} \tag{30}$$

The associated characteristic equation can be written in the form,

$$a_3 \lambda^3 + a_2 \lambda^2 + a_1 \lambda + a_0 = 0 \tag{31}$$

where a_0, a_1, a_2, and a_3 are functions of the stability and control derivatives. By applying *Routh-Hurwitz* stability criteria [20] as follows,

$$\begin{array}{c|cc} s^3 & a_3 & a_1 \\ s^2 & a_2 & a_0 \\ s^1 & B & \\ s^0 & a_0 & \end{array} \tag{32}$$

The number of sign changes in the second column of Eq. (32) will be the number of non-negative poles of the system in Eq. (30). The expressions for a_0, a_1, a_2, a_3 and B can be written in the following,

$$a_3 = 1 \tag{33}$$

$$a_2 = -X_u - M_q + g Z_u / (k_{w_0} Z_{\theta_{ls}} U_e) \tag{34}$$

$$a_1 \approx U_e M_{\theta_{ls}} Z_w / Z_{\theta_{ls}} - g Z_u M_q / (k_{w_0} U_e Z_{\theta_{ls}}) \tag{35}$$

$$a_0 \approx -g M_{\theta_{ls}} Z_u / Z_{\theta_{ls}} + M_u g Z_w / (k_{w_0} Z_{\theta_{ls}}) \tag{36}$$

and,

$$B = b_1 k_{w_0}^2 + b_2 k_{w_0} + b_3 \tag{37}$$

Eqns. (35) and (36) have been simplified. In Eq. (37), where the denominator a_2 has been ignored, the terms b_1, b_2, and b_3 are also functions of the stability and control derivatives. Their simplified expressions are shown as follows:

$$b_1 \approx ((-X_u - M_q) M_{\theta_{ls}} Z_w \cdot Z_{\theta_{ls}} U_e^3 \tag{38}$$

$$b_2 \approx M_{\theta_{ls}} g Z_u Z_w U_e^2 \tag{39}$$

$$b_3 = -g^2 Z_u^2 M_q \tag{40}$$

The analysis has shown that the expressions in Eqns. (34) and (35) are always positive. Moreover, the condition to guarantee a positive a_0 is shown as follows,

$$k_{w_0} < \frac{M_u Z_w}{Z_u M_{\theta_{ls}}} \tag{41}$$

This expression is exactly the same as that directly derived for the stability of the surge mode in Eq. (28). Therefore, the sign of a_0 is related to the stability of the surge mode.

The matrix in Eq. (30) consists of the surge and phugoid modes. Therefore, as far as the *Routh-Hurwitz* stability criteria are concerned, the stability variations or the crossing of the imaginary axes of the phugoid mode are hidden in the sign changes of Eq. (37). The sign variation can be analysed by the roots of Eq. (37) or $\Delta = b_2^2 - 4b_1b_3$. After simplification, the Δ equation, or generalised damping, can be expressed as follows

$$\Delta' \approx -M_{\theta_{ls}} Z_w U_e + 4Z_{\theta_{ls}} M_q^2 \qquad (42)$$

In addition, the Δ' values of the all cases being investigated are plotted in Fig. 8.

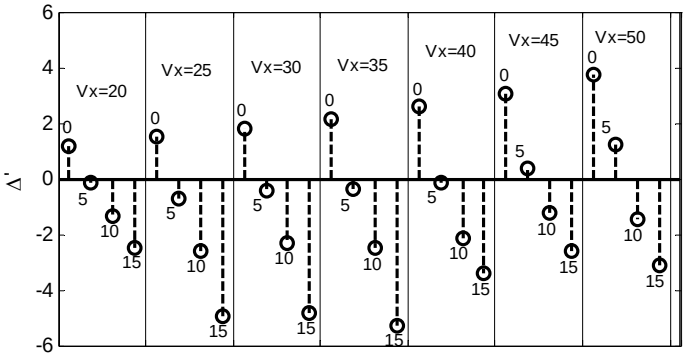

Fig. 8 Illustration of the generalised damping values (Δ') to show stability of the phugoid mode (the superscript numbers are the vertical speeds, kts)

In Fig. 8, the points above the data corresponding to $\Delta' > 0$ imply that the phugoid mode has two stability crossing points. The points corresponding to $\Delta' < 0$ imply that the phugoid mode has no crossing point. The locations of the points in Fig. 8 for all cases are consistent with the results presented in Figs. 1 and 2. For instance, the case of V_x =50 kts has two points corresponding to $\Delta' > 0$ which represent V_z = 0 kts and 5 kts, respectively - Figs. 2a and 2b show that there are, indeed, two crossing points. Overall, all these results have validated the derivation of Eq. (42).

Assuming that Eq. (37) [Eq. (42) positive] has two different roots K_1 and K_2 ($K_1 < K_2$) for stability changes, the following observations can then be made.

$0 < k_{w_0} < K_1$, phugoid mode stable (43)

$K_1 < k_{w_0} < K_2$, phugoid mode unstable (44)

$k_{w_0} > K_2$, phugoid mode stable (45)

The consistency between Eq. (41)/Fig. 8 and the original results shows the effectiveness of the applied WCS method. However, the primary drawback is that the method can only predict two stability crossings. Effectively, the initial point of the phugoid mode is assumed to be located in the stable plane. As a result, the first stability change is ignored, although the corresponding gains are very small and thus it is still illuminating to apply this approach in practice. This statement can be validated by calculating the critical values for the phugoid mode from the 'exact' matrix, as shown in Tables 2 and 3.

Table 2 Critical gains for the phugoid mode (exact matrix, deg/(m/s))

V_z = 0 kts\V_x	20 kts	25 kts	30 kts	35 kts	40 kts	45 kts	50 kts
K_1	0.0984	0.0984	0.0656	0.0656	0.0328	0.0328	0.0000
K_2	1.5751	1.2798	1.1814	1.0174	0.8861	0.8205	0.6891
K_3	55.722	45.910	36.361	30.453	25.892	22.315	20.149

Note: 0.0000 means the initial point for the phugoid model is located on the left-hand plane or neutrally stable

Table 3 Critical gains for the pitch attitude mode (exact matrix; deg/(m/s))

$V_z \backslash V_x$	20 kts	25 kts	30 kts	35 kts	40 kts	45 kts	50 kts
5 kts	0.0984	0.0328	0.0328	0.0328	0.0000	0.0000	×
10 kts	0.0328	0.0000	0.0000	0.0000	0.0000	0.0000	0.0000
15 kts	0.0000	0.0000	0.0000	0.0000	0.0000	0.0000	0.0000

Note:* × - *this case also has three critical gain values: 1.) 0 (neutral stable); 2.) 1.5752; and 3.) 2.7566

Table 2 shows the critical gains for level flight cases that generally have three intersecting point with the imaginary axis (the phugoid is unstable initially). In addition, as shown in this table, the gain values of the first intersecting point are all less than 0.1 deg/(m/s). Table 3 contains results for the descending flight cases. Compared with the level flight, the situation is more straightforward, since all curves are wholly located on the left-half plane or only have one intersecting point with the imaginary axis; an exception is the case of V_x = 50 kts and V_z = 5 kts. Moreover, even the gain values of the only intersecting point are also all less than 0.1 deg/(m/s).

With strong control of vertical velocity or flight path, the modes dominated by the uncontrolled speed and pitch attitude motions are intimately linked. Referring to Eq. (28), the larger the ratio M_u/Z_u, the higher the gain that can be used before the surge mode destabilises, but the earlier the phugoid mode transitions back into the unstable plane. For the case of the level flight with V_x = 30 kts, the gain value needed to guarantee surge mode stability is less than 0.5254 deg/(m/s) as shown in Table 1. In order to achieve the stability of the phugoid mode, the gain should be located within the range (0.0656, 1.1814) or larger than 36.361. Therefore, the gain selected from the interval (0.0656, 0.5254) will result in the combined system in Eq. (16) being stable.

The consequences of this complex interaction have been explored in an exploratory piloted simulation trial, reported in the following section.

6. Piloted simulation tests

6.1 Simulation objectives and mission task element

To investigate the potential RPCs and stability problems arising from the conflict between attitude control and flight-path control, a series of experiments have been initiated on the moving base HELIFLIGHT simulator at The University of Liverpool [19]. The simulation model used was the nonlinear FLIGHTLAB Bell 412. As previously discussed, the normal piloting strategy at low speed is to use collective for flight path control and cyclic for speed and attitude control. However, in this experiment, in order to tighten up the flight-path control, only the longitudinal cyclic was used. The situation is more similar to autorotation or where collective pitch is inhibited in some way. During the tests, the pilot(s) performed a series of approach-to-helipad profiles, with disturbance initiated at some points of the manoeuvres. This allowed for an investigation of the effects of different levels of task severity on pilot workload within defined performance standards. The test course is shown in Fig. 9.

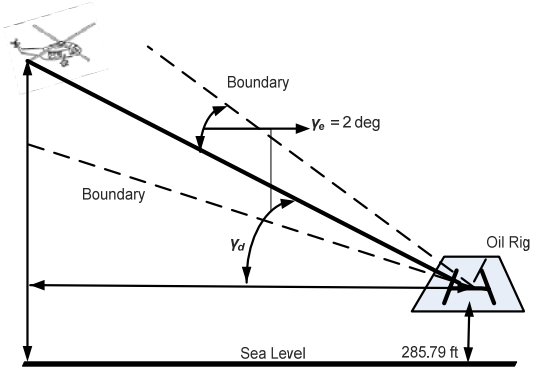

Fig. 9 Trajectory for investigation of flight-path constraint

To fly the course in Fig. 9, the pilot has to maintain the navigation error within the boundaries shown.

6.2 Analysis of results

Typical results from the piloted simulation trials are shown in Figs. 10 – 12.

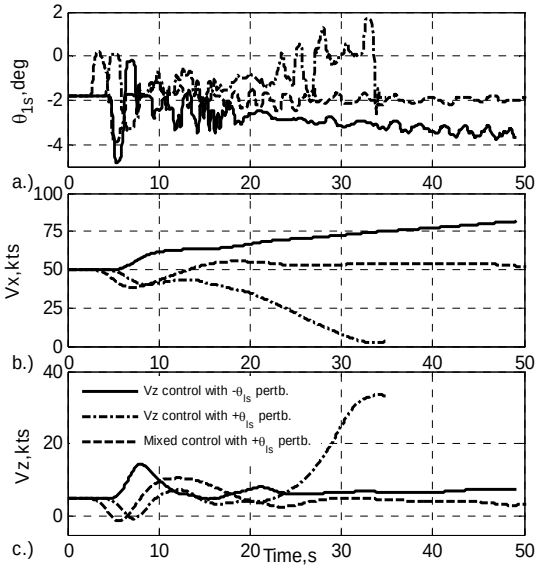

Fig. 10 Results of the piloted simulation (*Vx* = 50 kts and *Vz* = 5 kts)

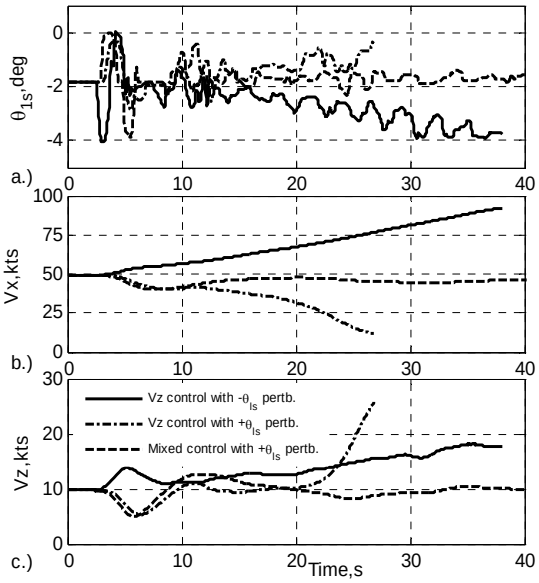

Fig. 11 Results of the piloted simulation (*Vx* = 50 kts and *Vz* = 10 kts)

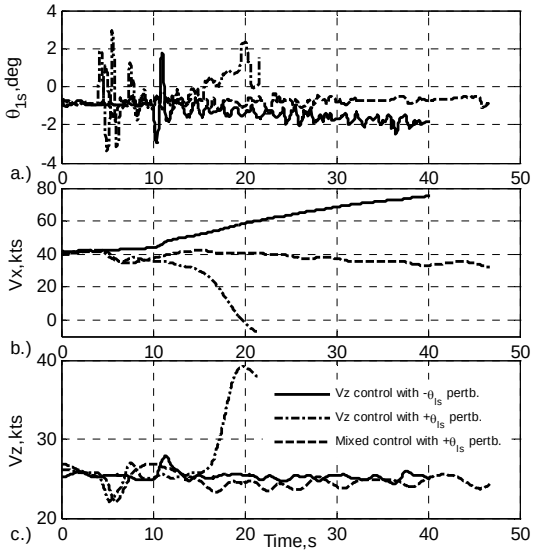

Fig. 12 Results of the piloted simulation (Autorotation, *Vx* = 50 kts)

In all three cases, results for three different situations are shown – a pitch down perturbation (-ve θ_{1s}) with pilot controlling vertical rate, a pitch up perturbation (+ve θ_{1s}) with pilot controlling vertical rate, and a pitch up perturbation with the pilot using a combined vertical rate and forward velocity control strategy. Fig. 10 corresponds to the 50kts partial power case with an initial glide slope of approximately 6 deg. Fig. 11 shows the aircraft at 50 kts with an initial glide slope of approximately 12 deg descent and Fig. 12 shows the autorotation case with a descent rate of about 2500 ft/min. The pattern is similar in all three-flight cases. With the pitch down perturbation, the pilot struggles to maintain rate of descent as the horizontal velocity component increases to more than 80kts. Following the pitch up perturbation, the horizontal velocity falls sharply and the pilot is soon unable to control the flight path as the rate of descent builds to over 3000 ft/min. Both of these cases are a consequence of the surge mode instability highlighted in Fig. 2. The linear approximation used to predict the behaviour in Fig. 2 breaks down of course when the velocity increases/decreases by more than a 'small' perturbation for the 50 kts trim condition. The oscillatory cyclic control pattern at about 2 rad/sec, clear in Fig. 11 but less so in Figs. 10 and 12, echoes the poorly damped closed loop phugoid mode in Fig. 2. Using a

mixed control strategy, combining control of horizontal and vertical speed, the pilot successfully maintains the flight condition in all three cases. The pilot referred to using much lower gain in this case and, closing the loop on airspeed, found that control of vertical rate was sometimes 'counter-intuitive' – pushing forward to climb and vice-versa. The non-minimum nature of vertical rate response to cyclic at low speed contributes to this effect, as discussed earlier in the paper.

7. Conclusions

This paper has documented results from an investigation into the RPC susceptibility for rotorcraft under flight path constraint. The main conclusions are summarised as follows:

Firstly, building on the foundation work of Ref [9], this is believed to be the first reported investigation of RPCs for descending flight situations with flight path constraint. Furthermore, a mathematical technique has been developed to predict this kind of RPC by taking into account the conflict between the controls of the speed and pitch attitude when the vertical speed feedback gain increases. The consequent results from the piloted simulation trials have validated this theoretical prediction. The flight simulation results also show that the pilot was able to learn a new technique to maintain the descent profile at low speed, even in autorotative flight.

Secondly, the theory of weakly coupled systems has been successfully adopted to facilitate understanding of the physical mechanisms of Cat. I RPCs, by partitioning the whole system into various levels of interacting subsystems. The drawbacks and limitations of different partitioning approaches have been compared and analysed. The three-level partitioning predicts the high gain limit of the phugoid mode and the two-level partitioning predicts the behaviour at low gain. A stability analysis, based on Routh-Hurwitz metrics has revealed the complex development of the phugoid stability under flight path constraint.

Thirdly, the critical values from the approximate surge mode, derived from the three-level partitioning, have been validated through comparison with the 'exact' closed-loop system.

Fourthly, the results from the piloted simulation trials in level flight, in powered descent and in autorotation all show, to varying degrees, the propensity for RPCs as the pilot controls flight path with cyclic. There is a close analogy with the earlier predictions on speed stability for fixed-wing aircraft flying below minimum drag speed. For a helicopter, the added complication is the presence of the phugoid mode driven by the large value of the aerodynamic derivative M_u, and the attendant risk of a combination of oscillatory and aperiodic divergent RPCs.

Acknowledgements

The research reported in this paper is funded by the UK Engineering and Physical Sciences Research Council grant EP/D003512/1 (Rotorcraft-Pilot Couplings). The study is also part of Liverpool's contribution to GARTEUR H-AG16, Rotorcraft Pilot Couplings. The FLIGHTLAB Bell 412 simulation model was created and validated from data provided by the Flight Research Laboratory of the Canadian National Research Council, Ottawa, as part of an ongoing collaboration in rotorcraft modelling, handling qualities and flight control. Grateful thanks are extended to the project test pilot, Andy Berryman for his contributions to the research.

References

1. McRuer, D.T., et al.. *Aviation Safety and Pilot Control Understanding and Preventing Unfavorable Pilot-Vehicle Interactions*, ASEB National Research Council, National Academy Press, Washington D.C., 1997.
2. Mitchell, D.G., and Klyde, D.H. Identifying a PIO signature – new techniques applied to an old problem, *J Guidance, Control and Dynamics*, Jan. 2008, **31**, (1), pp 215-225.
3. Klyde, D.H., and Mitchell, D.G. Investigating the role of rate limiting in pilot-induced oscillations, *J Guidance, Control and Dynamics,* Sept. 2004, **27**, (5), pp 804-813.

4. Padfield, G.D., Lawrence, B. The birth of the practical aeroplane; an appraisal of the Wright Brothers' achievements in 1905, *The Aeronautical Journal of the RAeS*, Oct. 2005, **109**, (110), pp 421-438
5. Shafer, M.F., and Steinmetz, P. Pilot-induced oscillation research status at the end of the century, NASA Dryden Flight Research Centre, Tech. Rep., Apr. 2001.
6. Hamel, Peter G. rotorcraft–pilot couplings. a critical issue for highly augmented helicopters?, Paper presented at the FVP Symposium an Advances in Rotorcraft Technology, AGARD CP-592, Ottawa, Canada, 27-30 May 1996.
7. Pavel, M.D., and Padfield, G.D. Understanding the peculiarities of rotorcraft-pilot couplings, Proc. 64th Annual Forum of the American Helicopter Society, Montreal, May 2008.
8. Walden, R.B. A retrospective survey of pilot-structural coupling instabilities in naval rotorcraft, 63rd Annual Forum of the American Helicopter Society, Virginia Beach, VA, May 1-3, 2007.
9. Padfield, G.D., *Helicopter Flight Dynamics,* 2nd edition, Blackwell Science, Oxford, 2007.
10. Masarati, P., Quaranta, J., and Serafini, M. Numerical Investigation of aeroservoelastic rotorcraft-pilot coupling, XIX Congresso AIDAA, Forlì, Italy, Sept. 2007.
11. Koivo, A.T., Repperger, D.W., and Koivo, A.J. Detection of aircraft-pilot-coupling caused oscillations, Proceedings of IEEE International Symposium on Computational Intelligence in Robotics and Automation, CIRA '99, Nov. 1999
12. Neumark, S. Problems of longitudinal stability below minimum drag speed, and theory of stability under constraint, Aeronautical Research Council, R&M 2983, HMSO London, Jul. 1953.
13. Pinsker, W.J.G. Glide-Path Stability of an Aircraft under Speed Constraint", Aeronautical Research Council, R&M 3705, HMSO London, Feb. 1971.
14. Milne, R.D., and Padfield, G.D. The strongly controlled aircraft, *Aeronautical Quarterly*, May 1971, **XXII**, (2), pp 146-168.
15. Hodgkinson, J., Glessner, P.T., and Mitchell, D.G. Prediction of longitudinal pilot-induced oscillations using a low order equation system approach, NASA/CP-2001-210389/VOL2, pp 67-80, Apr. 2004
16. Hess, R.A., and Kalteis, R.M. Technique for predicting longitudinal pilot-induced oscillations, *J Guidance, Control and Dynamics*, 1991, **14**, (1), pp 198-204.
17. Manimala, B.J., Walker, D.J., Padfield, G.D., Voskuijl, M., Gubbels, A.W. Rotorcraft simulation modelling and validation for control law design, *The Aeronautical Journal of the RAeS*, Feb. 2007, **111**, (1116), pp 77-88.
18. Milne, R.D. The analysis of weakly coupled dynamic systems, *International Journal of Control*, Aug. 1965, **2**, pp 171-199.
19. Padfield, G.D., White, M.D. Flight simulation in academia; HELIFLIGHT in its first year of operation, *The Aeronautical Journal of the Royal Aeronautical Society*, Sept. 2003, **107**, (1075), pp 529-538.
20. Duncan, W.J. The Principles of the Control and Stability of Aircraft, Cambridge University Press, 1952.